fibers

MDPI

Article

Influence of Geometric Non-Linearities on the Mixed-Mode Decomposition in Asymmetric DCB Samples

Jorge Bonhomme [1,*], Victoria Mollón [2], Jaime Viña [2] and Antonio Argüelles [1]

[1] Department of Construction and Manufacturing Engineering, University of Oviedo, 33203 Gijón, Spain; antonio@uniovi.es
[2] Department of Materials Science and Metallurgical Engineering, University of Oviedo, 33203 Gijón, Spain; mollonvictoria@uniovi.es (V.M.); jaure@uniovi.es (J.V.)
* Correspondence: bonhomme@uniovi.es

Abstract: The Asymmetric Double Cantilever Beam (ADCB) is a common test configuration used to produce mixed mode I/II in composite materials. It consists of two sublaminates with different thicknesses or elastic properties, a situation that usually occurs in bimaterial adhesive joints. During this test, the sample undergoes rotation. In this work, the influence of this rotation on the calculation of the energy release rate (ERR) in modes I and II was studied using the Finite Element Method (FEM). Several models with different degrees of asymmetry (different thickness ratio and/or elastic modulus ratio) and different applied displacements were prepared to obtain different levels of rotation during the test. As is known, the concept of modes I and II refers to the components of the energy release rate calculated in the direction perpendicular and tangential to the delamination plane, respectively. If the model experiences significant rotation during the application of the load, this non-linearity must be considered in the calculation of the mode partition I/II. In this work, appreciable differences were observed in the values of modes I and II, depending on their calculation in a global system or a local system that rotates with the sample. When performing crack growth calculations, the difference between critical loads can be in the order of 4%, while the difference between mode I and mode II results can reach 4% and 14%, respectively, for an applied displacement of only 5 mm. Currently, this correction is not usually implemented in Finite Element calculation codes or in analytical developments. The purpose of this article is to draw attention to this aspect when the rotation of the specimen is not negligible.

Keywords: FEM; composite laminate; interlaminar fracture toughness; mixed mode; delamination; CFRP; ADCB

check for updates

Academic Editors: Michela Simoncini and Archimede Forcellese

Received: 10 April 2025
Revised: 8 May 2025
Accepted: 22 May 2025
Published: 27 May 2025

Citation: Bonhomme, J.; Mollón, V.; Viña, J.; Argüelles, A. Influence of Geometric Non-Linearities on the Mixed-Mode Decomposition in Asymmetric DCB Samples. *Fibers* **2025**, *13*, 70. https://doi.org/10.3390/fib13060070

Copyright: © 2025 by the authors. Licensee MDPI, Basel, Switzerland. This article is an open access article distributed under the terms and conditions of the Creative Commons Attribution (CC BY) license (https://creativecommons.org/licenses/by/4.0/).

1. Introduction

Delamination failure is a critical factor limiting the service life of fibre-reinforced thermoset matrix composites, as they are composed of laminated layers. Crack initiation and growth in these materials can occur under loading modes I, II and III. However, in most practical applications, a combination of these modes is typically observed.

Standardized test configurations have been developed for characterizing fracture under pure modes I and II. The Double Cantilever Beam (DCB) test is the established method for pure mode I, while the End Notch Flexure (ENF) test is commonly used for pure mode II. These procedures have been elevated to international standards [1–3]. Regarding mode III, there is, so far, no consensus to establish any test procedure as an international standard.

Among mixed-mode loading scenarios, mode I/II has received significant attention in research. The standardized Mixed-Mode Bending (MMB) test method is widely used to generate a combination of modes I and II at the crack tip [4,5]. In this test configuration, mode I is introduced by means of an opening movement as in the DCB test, and mode II is produced by means of the specimen flexure (as in the ENF test) (see Figure 1).

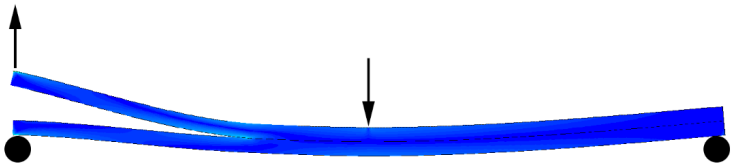


Figure 1. MMB tests (Mixed-Mode Bending). Arrow-up: opening load. Arrow-down: bending load.

Other test methods to obtain mixed modes I/II are based on the ENF test, such as the Single Leg Bending (SLB), the Asymmetric Single Leg Bending (ASLB) tests [6,7] and the Prestressed End Notched Flexure (PENF) test (Figure 2). In the PENF test configuration, proposed by Szekrényes [8], mode I is introduced by means of a rod inserted between both sublaminates, and mode II is produced by the specimen flexure. This test is simple to perform, as it eliminates the need for bonding hinges to the sample. Boyano et al. studied the influence of different rod positions and diameters on the mixed mode at the crack tip [9].

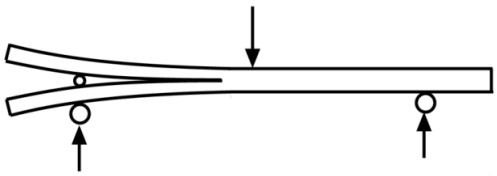


Figure 2. Prestressed End Notched Flexure (PENF) test. Arrows-up: reaction loads. Arrow-down: applied load.

The Asymmetric Double Cantilever Beam (ADCB) test offers another alternative to generate mixed mode I/II [10–12] (see Figure 3). In this configuration, both sublaminates have different stiffnesses. This is the situation when the sublaminates have different thicknesses and/or different elastic properties (e.g., bimaterial bonded joints). The ADCB test generates a mixed mode I/II at the crack tip with predominance of mode I, and its specimens and fittings maintain the simplicity of pure mode I (DCB) tests. As can be seen in Figure 3, as the load is applied to the test specimen, the ADCB sample rotates due to the different stiffnesses of the sublaminates.

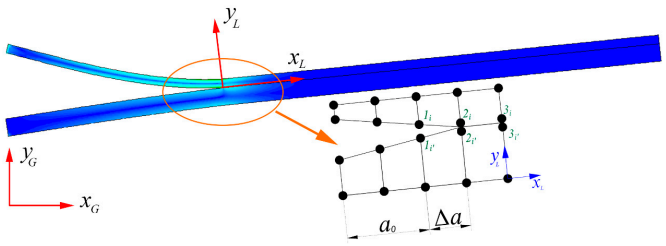


Figure 3. ADCB specimen and mesh at the crack tip with local (x_L-y_L) and global (x_G-y_G) coordinate systems.

The mixed-mode delamination process has also been extensively studied via numerical and analytical calculations. The numerical calculation of delamination is usually carried out using the Virtual Crack Closure Technique (VCCT) [13] and the Cohesive Zone Modelling (CZM) [14,15] available in commercial FEM programs. VCCT numerical calculations are

usually carried out in global coordinates, without taking into account the possible rotation of the specimen during the test as in the ADCB specimen (Figure 3).

The analytical developments are also usually performed in global coordinates without considering the geometrical non-linearity introduced by the rotation of the delamination plane. The analytical determination of the ERR decomposition in modes I and II (G_I and G_{II}) is not simple when the mixed mode is present at the crack tip. There are several methods developed in the scientific literature to evaluate mode I/II partition, but there is not always consensus among researchers [12,16–18].

This article aims to draw attention to the fact that, when the ADCB specimen rotates in a non-negligible way during the test (see Figure 3), not taking said rotation into account in the projection of the forces and displacements can give rise to an appreciable error in the decomposition of modes I and II. This study is limited to the calculation of the ERR using FEM, although the conclusions drawn can be extrapolated to analytical calculation procedures. This study is also limited to linear elastic materials. Linear Elastic Fracture Mechanics (LEFM) was assumed throughout this study.

2. Materials and Methods

In this work, the ANSYS® 2024 Academic Research package was used to study the influence of the specimen rotation on the ERR decomposition in modes I and II in ADCB specimens via FEM.

As mentioned above, the concept of modes I and II refers to the components of the energy release rate calculated in the direction perpendicular and tangential to the delamination plane, respectively. To correctly calculate G_I and G_{II}, the components of the forces and displacements involved in the energy calculation must be projected in directions perpendicular and tangential to the delamination plane (x_L-y_L coordinate system) (see Figure 3).

In this study, two coordinate systems are defined: a global coordinate system (GCS) (x_G-y_G), with the x_G-axis aligned with the crack plane when the specimen is unloaded that remains horizontal during the test, and a local coordinate system (LCS) (x_L-y_L) that rotates with the crack plane while loading the sample. Therefore, the x_L-axis is always aligned with the crack during the test (see Figure 3).

If the rotation of the specimen during the test is significant, the difference in the calculations obtained using both coordinate systems may be non-negligible. As shown in Figure 3, during the ADCB test, when the sublaminates have a significant difference in stiffness, an appreciable rotation of the specimen occurs.

To carry out this study, several ADCB models were prepared with different thickness ratios (h_1/h_2) in order to obtain different degrees of modes I/II (see Figure 4).

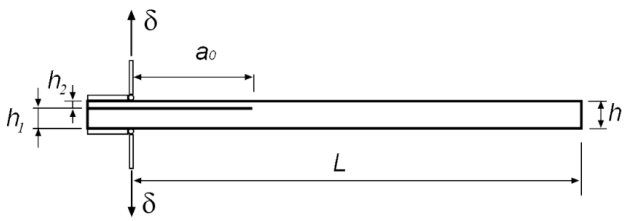


Figure 4. ADCB. Specimen configuration.

A constant displacement δ was applied to all models on the sample lips (see Figure 4). G_I and G_{II} were then calculated using forces and displacements in global and local coordinates.

FEM packages usually implement the Virtual Crack Closure Technique (VCCT) in order to calculate G_I and G_{II}. The VCCT method calculates the energy released by the opening of the nodes during crack growth in a single step. This is a simplification since

the force is calculated at the crack tip when the crack has already grown, but it is a very efficient calculation method.

In the VCCT method [13] (see Figure 5), the components of forces and displacements are calculated in the same step using two different node pairs. Forces are calculated in nodes *2i-2i'*, and displacements are calculated in nodes *1i-1i'*. This approximation is valid providing that forces at the crack tip before and after the crack extension are similar when the crack increment (element size) is small enough.

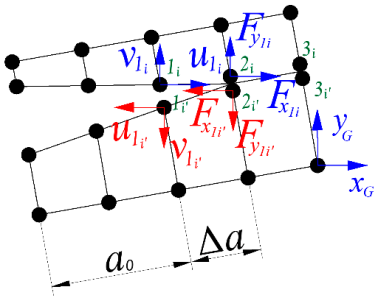


Figure 5. VCCT method in global coordinate system.

The calculation using the VCCT method was performed with the CINT function of the ANSYS program (CINT,TYPE,VCCT) [19].

G_I and G_{II} are then calculated as follows:

$$G_I = \frac{1}{2B\Delta a}\sum_{i=1}^{n} F_{y2i}(v_{1i} - v_{1'i}) \quad (1)$$

$$G_{II} = \frac{1}{2B\Delta a}\sum_{i=1}^{n} F_{x2i}(u_{1i} - u_{1'i}) \quad (2)$$

B is the specimen width. The subscript i takes into account a 3D system with n nodes along the crack front.

The VCCT method, implemented in this commercial FEM package, uses the global coordinate system to perform the calculations (the coordinate system is not updated as the crack plane rotates).

In this article, a similar method without simplification (TSEM) is also used. In this method, loads are calculated in the first step, and the corresponding displacements are calculated in a second step once the nodes have separated. Loads and displacements are, therefore, calculated in the same node pair (nodes *1i-1i'* in Figures 6 and 7) [20,21].

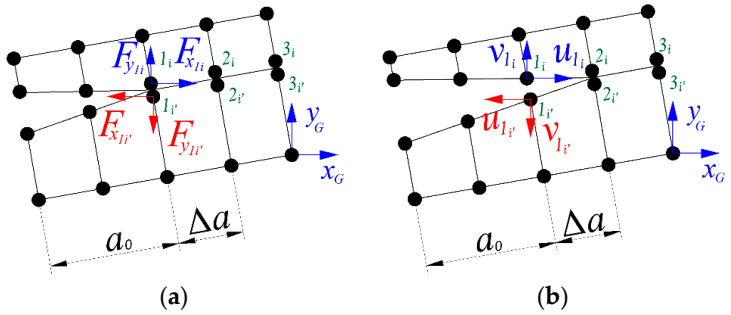
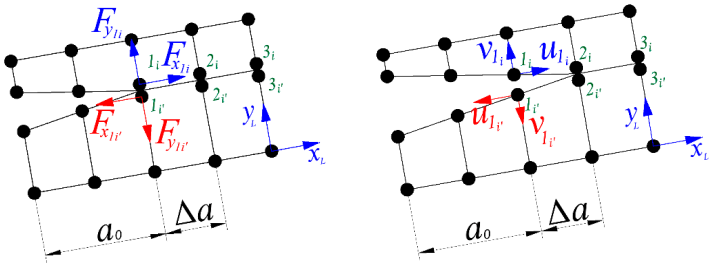


Figure 6. TSEM method in global coordinate system. (**a**) Step 1. (**b**) Step 2.



(**a**) (**b**)

Figure 7. TSEM method in local coordinate system. (**a**) Step 1. (**b**) Step 2.

G_I and G_{II} are calculated by means of TSEM as follows:

$$G_I = \frac{1}{2B\Delta a}\sum_{i=1}^{n} F_{y1i}(v_{1i} - v_{1'i}) \tag{3}$$

$$G_{II} = \frac{1}{2B\Delta a}\sum_{i=1}^{n} F_{x1i}(u_{1i} - u_{1'i}) \tag{4}$$

Therefore, data need to be collected in two successive calculation steps to perform the energy calculations. This method was applied using both global (Figure 6) and local coordinate systems (Figure 7).

This method is not originally implemented in the ANSYS FEM package. Therefore, a script programmed in APDL (Ansys Parametric Design Language) was specifically developed for this purpose in this work. This method was programmed using local and global coordinates. In this way, it will be possible to compare results taking, or not, into account the rotation of the coordinate system. Moreover, TSEM results in global coordinates can be compared with the VCCT originally implemented in ANSYS (and most commercial FEM packages), as they are equivalent when the element size ahead of the crack tip is small enough.

The material used to perform this study is a unidirectional carbon/epoxy laminate AS4/8552. The mechanical properties of this laminate taken from [22] are shown in Table 1. The Poisson coefficient ν_{yz} has been calculated as isotropic.

Table 1. Mechanical properties of laminate AS4/8552.

Property	AS4/8552
E_x (MPa)	144,000
E_y (MPa)	10,600
E_z (MPa)	10,600
G_{xy} (MPa)	5360
G_{xz} (MPa)	5360
G_{yz} (MPa)	3786
ν_{xy}	0.34
ν_{xz}	0.34
ν_{yz}	0.40
G_{Ic} (N/mm)	0.250
G_{IIc} (N/mm)	0.791

3. Model Calibration

A 2D FEM model was prepared using ANSYS® 2024 Academic Research. The element used was the 2D 4-node structural solid PLANE182 with full integration, plane strain behaviour and pure displacement formulation options.

A first model was prepared to optimize the element size near the crack tip. This model had the following dimensions:

- L = 150 mm
- a_0 = 50 mm
- h_1 = 4.6 mm
- h_2 = 1.4 mm

A regular mesh was implemented with the same size before and after the crack tip (Figure 8).

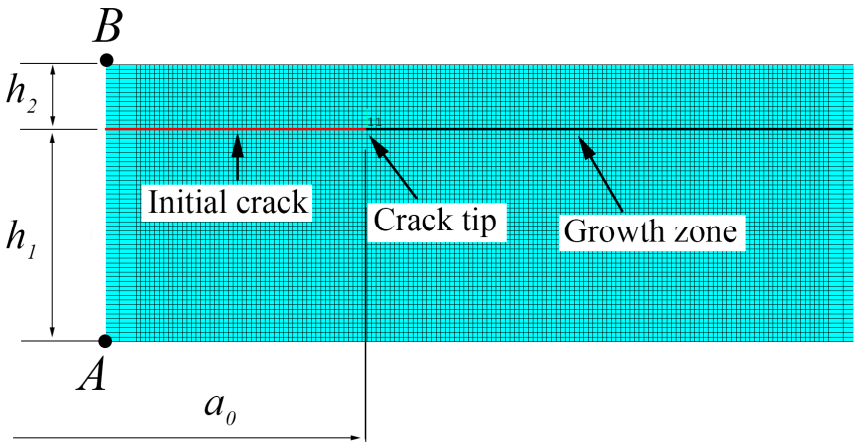


Figure 8. Mesh near the crack tip.

A displacement of δ = 8 mm was applied to the sample lips. The boundary conditions were set as follows:

- $u_A = v_A = 0$
- $u_B = 0$, $v_B = \delta$

Both TSEM and VCCT procedures were used in this study. In order to apply the TSEM procedure, an APDL script was prepared with the crack path modelled by coupling the degrees of freedom of coincident nodes from the upper and lower sublaminates ahead of the crack tip. The crack growth is then produced by releasing the node set at the crack tip when the critical displacement is imposed (see Figures 6 and 7). When using the standard VCCT procedure implemented in ANSYS (Figure 5), the CINT function of the ANSYS program [19] was used.

Several runs using the TSEM procedure were performed in global coordinates with different element sizes to optimize the model. The mesh was refined around the crack tip until variation in the results was negligible. The elements were nearly squared. Finally, the element size in the vicinity of the crack tip was set to 0.100 mm for the following studies. A thinner mesh would produce a negligible change in ERR values (0.1%).

Another issue to take into consideration is whether the calculations should be performed in a linear or non-linear way due to sample rotation.

To perform VCCT crack growth simulations, the ANSYS manual specifies the assumption that the model undergoes a small deformation (or a small rotation), and so, the calculation is performed with the option NLGEOM, OFF [19]. This option causes the calculation to be performed via a linear procedure, without taking into account possible non-linear effects. There are three possible sources of non-linearities: material non-linearity, contacts and large displacements or deformations. This is an issue to take into account, as asymmetric specimens may show non-negligible rotations.

Large displacements or rotations can cause the stiffness of the system to change as the load is applied to the sample lips. If the change in the stiffness of the system during the

loading process is not negligible, it must be taken into account as a source of non-linearity in the calculations.

Two runs were performed to investigate the influence of the calculation procedure (linear or non-linear procedure).

The model used was the same as the one used for element size optimisation. In this case, a displacement of 4.5 mm was applied to the sample. This displacement is assumed to be close to the critical displacement of the material for this configuration. The obtained results are shown in Table 2.

Table 2. Linear and non-linear calculations. TSEM procedure.

Solution Procedure	P (N)	G_I (N/mm)	G_{II} (N/mm)	G_T (=G_I + G_{II}) (N/mm)	G_T ($-dU/(Bda)$) (N/mm)	%G_I	%G_{II}
Linear	2.985	0.288	0.093	0.382	0.382	76%	24%
Non-linear	3.008	0.282	0.102	0.384	0.385	74%	26%

The units of the applied load were set as N, assuming a width of 1 mm (a 2D model was used). In Table 2, the total energy release rate (G_T) is calculated in two ways: as the sum of G_I and G_{II} previously calculated by means of the TSEM procedure, and, directly, by means of the overall loss of elastic energy divided by the area of the crack increment (one element length). It takes the following mathematical form:

$$G_T = -\frac{1}{B}\frac{dU}{da} \tag{5}$$

Both procedures give similar results (linear and non-linear), but, as can be seen in Table 2, linear calculations give identical results, irrespective of the procedure used to calculate G_T (0.382 N/mm).

This FEM model was also used to compare both TSEM solution procedures (linear and non-linear) with the analytical Corrected Beam Theory (CBT) proposed by the ISO 15024 [1] standard, equivalent to the Modified Beam Theory (MBT) in ASTM D 5528 [2]. Although this formulation is designed to calculate G_I in symmetric samples, it can also be used to calculate G_T in asymmetric samples, as demonstrated in [23].

$$G_T = \frac{3P\delta}{2B(a+\Delta)} \tag{6}$$

where

- P: applied load
- δ: applied displacement
- B: sample width
- a: crack length
- Δ: crack length correction

Δ takes into account that the beam is not perfectly built in. This parameter is calculated by plotting the cube-root of the compliance as a function of delamination length. The extrapolation of the linear fit through the data in the plot yields Δ as the x-intercept [1]. This was achieved by analysing various models with h_1 = 4.6 mm, h_2 = 1.4 mm and different initial crack lengths via FEM. Once Δ was obtained, a new model with a_0 = 50 mm and an applied displacement δ = 4.5 mm was analysed. Table 3 shows the obtained results calculated following Equations (3) and (4) and, additionally, with the analytical Equation (6). These calculations were performed using linear and non-linear solutions.

Table 3. Total energy release rate calculated by means of TSEM and analytical formulation (Equation (6)).

Calculation Procedure	G_T (N/mm) TSEM (Equations (3) and (4))	G_T (N/mm) Analytical CBT Equation (Equation (6))	Δ (mm)	Var. TSEM-Analytical
Linear	0.382	0.385	3.04	−0.4%
Non-linear	0.384	0.382	2.12	−0.2%

As can be seen in Table 3, both solution procedures (linear and non-linear) yield similar results and agree very well with the analytical CBT solution. The time needed to solve the model with each procedure is very similar since a 2D model is used.

Because the solution time is similar between the two procedures, a non-linear solution will be used in the following calculations to take into account the small non-linearities present in this model (the stiffness matrix of the model changes slightly as the displacement is applied).

4. Influence of the Sample Rotation

4.1. Rotation Due to the Applied Displacement

Once the model had been optimized, several runs were performed, increasing the applied displacement with the same model used in the previous studies. This caused the sample to progressively increase its rotation (see Figure 9). The aim of this study is to assess the influence of taking, or not, into account the sample rotation on the ERR calculations.

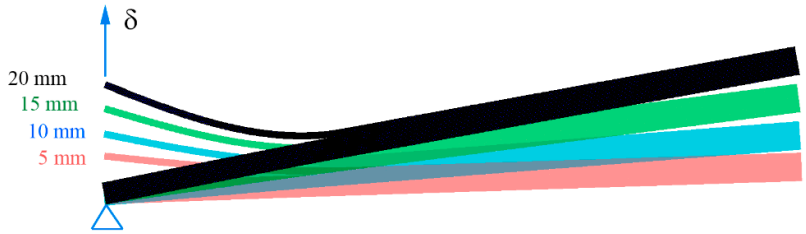


Figure 9. Deformed sample for different applied displacements. Sample configuration: a_0 = 50 mm, h_1 = 4.6 mm, h_2 = 1.4 mm. Elastic properties: Table 1.

These models were analysed using TSEM in local and global coordinates (i.e., taking or not into account sample rotation on ERR calculation) by means of an APDL script developed specifically for this purpose and, also, using the VCCT procedure available in ANSYS by means of the CINT,TYPE,VCCT function. As commented before, this VCCT function, implemented in the ANSYS package, uses only global coordinates (rotation is not taken into account).

The results are shown in Tables 4–6.

Table 4. VCCT. Global coordinates. a_0 = 50 mm, h_1 = 4.6 mm, h_2 = 1.4 mm. Elastic properties in Table 1.

δ (mm)	P (N)	δ/P (mm/N)	G_I (N/mm)	G_{II} (N/mm)	G_T (N/mm)	G_I/G_T	G_{II}/G_T
1	0.664	1.506	0.014	0.005	0.019	75%	25%
5	3.347	1.494	0.348	0.127	0.476	73%	27%
10	6.802	1.470	1.332	0.586	1.919	69%	31%
15	10.404	1.442	2.854	1.523	4.376	65%	35%
20	14.254	1.403	4.825	3.117	7.942	61%	39%

Table 5. TSEM. Global coordinates. a_0 = 50 mm, h_1 = 4.6 mm, h_2 = 1.4 mm. Elastic properties in Table 1.

δ (mm)	P (N)	δ/P (mm/N)	G_I (N/mm)	G_{II} (N/mm)	G_T (N/mm)	G_I/G_T	G_{II}/G_T
1	0.664	1.506	0.014	0.005	0.019	75%	25%
5	3.347	1.494	0.347	0.127	0.474	73%	27%
10	6.802	1.470	1.335	0.587	1.922	69%	31%
15	10.404	1.442	2.866	1.528	4.394	65%	35%
20	14.254	1.403	4.856	3.135	7.991	61%	39%

Table 6. TSEM. Local coordinates. a_0 = 50 mm, h_1 = 4.6 mm, h_2 = 1.4 mm. Elastic properties in Table 1.

δ (mm)	P (N)	δ/P (mm/N)	G_I (N/mm)	G_{II} (N/mm)	G_T (N/mm)	G_I/G_T	G_{II}/G_T
1	0.664	1.506	0.014	0.005	0.019	76%	24%
5	3.347	1.494	0.363	0.112	0.474	76%	24%
10	6.802	1.470	1.486	0.436	1.922	77%	23%
15	10.404	1.442	3.431	0.963	4.394	78%	22%
20	14.254	1.403	6.297	1.694	7.991	79%	21%

Comparing Tables 4 and 5, we can see that both procedures yield practically identical results and match the partition values G_I/G_T and G_{II}/G_T. These results were as expected, as both procedures perform the calculations in global coordinates, and they are very similar, only differing in the node where the force is calculated (one element length away from each other) (see Figures 5 and 6). The two procedures tend to converge on each other as the size of the element at the crack tip decreases.

As can be seen in Tables 4 and 5, when the applied displacement δ is increased from 1 mm to 20 mm (the rotation of the sample increases), the partition value G_I/G_T varies from 75% to 61% and G_{II}/G_T varies from 25% to 39%. This represents a 19% change in the G_I/G_T value and a 56% change in the G_{II}/G_T value. This change in partition values can be attributed to the appreciable rotation of the sample as the displacement increases. It would be expected that the percentages would show a low variation as the applied displacement increases. However, in this case, since the rotation of the specimen is not taken into account in the projection of the forces and displacements in the ERR calculation, the error increases as the applied displacement increases. We must remember that, in Tables 4 and 5, forces and displacements are always calculated horizontal and vertical (according to the GCS) independent of the sample rotation.

On the other hand, Table 6 shows the calculation of the ERR using forces and displacements projected perpendicular and parallel to the crack plane, that is, considering the rotation of the sample (using an LCS that rotates with the crack plane). Using the LCS, the partition value G_I/G_T varies from 76% to 79% and G_{II}/G_T varies from 24% to 21% when the displacement applied to the sample is increased from δ = 1 mm to δ = 20 (this represents a 4% change in the G_I/G_T value and 13% change in the G_{II}/G_T value). As expected, the ERR partition based on LCS has a much smaller change due to rotation than in the previous ERR calculations based on GCS. Now, G_I and G_{II} are calculated perpendicular and tangential to the crack plane. In this case, the small change in the partition values as the sample rotates could be influenced, among other things, by the shortening of the distance a_0 due to sample rotation and arm flexure (Table 7 shows the crack tip displacement u_x for different applied displacements δ).

Table 7. TSEM. Change in the ERR values (G_I, G_{II} and G_T) in local and global coordinate systems. Superscript "L" denotes local coordinates and superscript "G" denotes global coordinates.

δ (mm)	$\frac{G_I^G - G_I^L}{G_I^L}$	$\frac{G_{II}^G - G_{II}^L}{G_{II}^L}$	$\frac{G_T^G - G_T^L}{G_T^L}$	Rotated Angle (Rad.)	Crack Tip Node u_x Displacement (mm)
1	−1%	2%	0%	0.0035	−0.022
5	−4%	14%	0%	0.0292	−0.196
10	−10%	35%	0%	0.0713	−0.571
15	−16%	59%	0%	0.1172	−1.116
20	−23%	85%	0%	0.1647	−1.836

Finally, as expected, the total energy G_T dissipated when the crack grows is the same for a given displacement, independent of the coordinate system used (Tables 5 and 6). Obviously, the total energy does not depend on the coordinate system used to calculate G_I and G_{II}.

We can evaluate the ERR modes I and II in global coordinates ($G^G{}_I$, $G^G{}_{II}$) as a function of modes I and II in local coordinates ($G^L{}_I$, $G^L{}_{II}$) (Figure 10) or vice versa as follows:

$$F_y^G = F_y^L \cos(\alpha) + F_x^L \sin(\alpha), \quad u_y^G = u_y^L \cos(\alpha) + u_x^L \sin(\alpha) \tag{7}$$

$$F_x^G = F_x^L \cos(\alpha) - F_y^L \sin(\alpha), \quad u_x^G = u_x^L \cos(\alpha) - u_y^L \sin(\alpha) \tag{8}$$

$$G_I^G = G_I^L cos^2\alpha + G_{II}^L sin^2\alpha + \frac{1}{2B\Delta a}\left(F_y^L \Delta u_x^L + F_x^L \Delta u_y^L\right) \sin(\alpha)\cos(\alpha) \tag{9}$$

$$G_{II}^G = G_I^L sin^2\alpha + G_{II}^L cos^2\alpha - \frac{1}{2B\Delta a}\left(F_y^L \Delta u_x^L + F_x^L \Delta u_y^L\right) \sin(\alpha)\cos(\alpha) \tag{10}$$

and adding Equations (9) and (10):

$$G_T = G_I^G + G_{II}^G = G_I^L + G_{II}^L \tag{11}$$

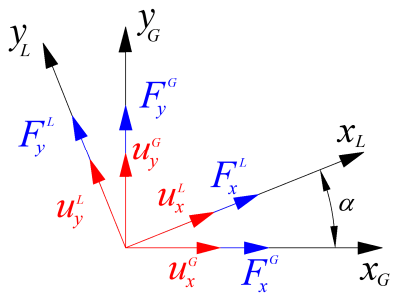


Figure 10. Coordinate transformation.

Table 7 shows the differences between the ERR values G_I, G_{II} and G_T calculated in GCS and LCS based on the results in Tables 5 and 6.

As expected, for small rotations, the difference between calculations in GCS and LCS is low, but if the rotation of the sample is significant, the error made when calculating in GCS can be very significant compared to LCS. For a displacement of only 5 mm, the difference obtained in G_I and G_{II} values is 4% and 14%, respectively, when calculating GCS and LCS. And, for a displacement of 10 mm, the differences in G_I and G_{II} values reach 10% and 35%, respectively.

In addition to sample rotation, as stated above, another source of non-linearity is the displacement of the crack tip node as the applied load increases (see Table 7). For δ = 20 mm, the equivalent crack length (measured perpendicular to the loading axis) shortens by 1.836 mm, making the sample response stiffer.

4.2. Rotation Due to the Degree of Asymmetry

Next, some models were prepared with different h_2/h_1 and E_{x2}/E_{x1} ratios in order to have different degrees of asymmetry so as to produce different mixity modes. These models were solved using the TSEM procedure in local and global coordinates.

The applied load was δ = 10 mm, and the initial crack length was a_0 = 50 mm for all models. The obtained results can be seen in Table 8.

Table 8. ERR partition values of several samples with different h_2/h_1 and E_2/E_1 rates. GCS: Global Coordinate System. LCS: Local Coordinate System. d = 10 mm. a_0 = 50 mm.

E_{x1}(MPa)	E_{x2}/E_{x1}	h_2/h_1	$\frac{E_{x2}h_2^2}{E_{x1}h_1^2}$	GCS $\%G_I$	GCS $\%G_{II}$	LCS $\%G_I$	LCS $\%G_{II}$	Rotated Angle (Rad.)
144.000	1	1.000	1.000	100%	0%	100%	0%	0
144.000	1	0.714	0.510	95%	5%	97%	3%	0.0323
144,000	1	0.500	0.250	84%	16%	88%	12%	0.0563
144,000	1	0.333	0.111	72%	28%	79%	21%	0.0697
144,000	1	0.200	0.040	62%	38%	71%	29%	0.0751
144,000	0.25	0.200	0.010	43%	57%	52%	48%	0.0812
144,000	0.125	0.200	0.005	39%	61%	48%	52%	0.0822

The ratio ${E_{x1}h_1}^2/{E_{x2}h_2}^2$ is included in Table 8 to give an idea of how far each configuration is from the pure mode I condition, assuming that the pure mode I condition is reached when the longitudinal strain distributions at both sublaminates interfaces are identical [24] (Figures 11 and 12). Therefore, the pure mode I condition is achieved as follows:

$$u_1 = u_2 \rightarrow \gamma_{xy} = 0 \tag{12}$$

$$\frac{du_1}{dx} = \frac{du_2}{dx} \rightarrow \varepsilon_1 = \varepsilon_2 \rightarrow \frac{Mh_1}{2E_{x1}I_1} = \frac{Mh_2}{2E_{x2}I_2} \rightarrow E_{x1}h_1^2 = E_{x2}h_2^2 \tag{13}$$

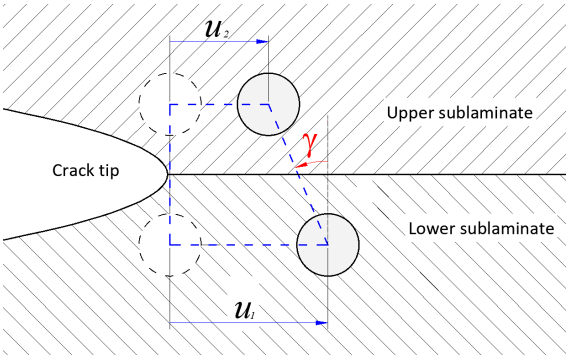


Figure 11. Displacement near the crack tip.

Figure 13 shows the rotation of the sample with h_2/h_1 = 0.2 compared to the symmetric sample for δ = 20 mm.

As can be seen in Table 8, as the degree of asymmetry increases, the difference between the calculated values in LCS and GCS increases. These results are consistent with previous findings, since the increase in the degree of asymmetry leads to an increase in sample rotation.

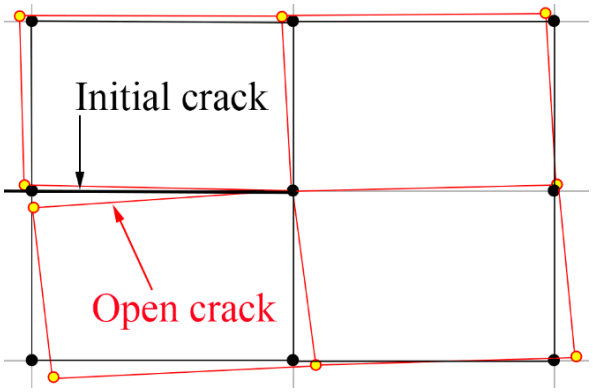


Figure 12. Mesh deformation near the crack tip.



Figure 13. Deformed sample for different sublaminate stiffness for an applied displacement of 20 mm. Sample configuration: a_0 = 50 mm. Elastic properties: Table 1.

4.3. Crack Growth Calculations

Finally, crack growth calculations were performed in order to evaluate the influence of the coordinate system used in the calculations (LCS or GCS) on the obtained critical load. These models were solved using TSEM in local and global coordinates.

To determine the crack onset and subsequent crack growth, it is necessary to define a fracture criterion. The Benzeggagh–Kenane criterion (B-K) was assumed [19,25]:

$$\frac{G_T}{G_{Ic} + (G_{IIc} - G_{Ic})\left(\frac{G_{II}}{G_T}\right)^{\eta}} \geq 1 \tag{14}$$

The exponent η was set at 1.45, following [26].

The elastic properties and critical values G_{Ic} and G_{IIc} of both sublaminates were taken from Table 1. Other parameters were as follows:

- h_1 = 5 mm
- h_2 = 1 mm
- a_0 = 50 mm

The obtained results are shown in Table 9. Figure 14 shows the corresponding load–displacement curves. As can be seen in Table 9, the difference between critical values (both load and displacement) is in the order of 4% in this case. The calculation performed in the LCS is on the safe side as it predicts the onset of crack growth at lower load and displacement.

Table 9. Crack onset critical values in global (GCS) and local (LCS) coordinates.

	δ_c (mm)	P_c (N/mm)
GCS	6.99	1.832
LCS	6.74	1.765

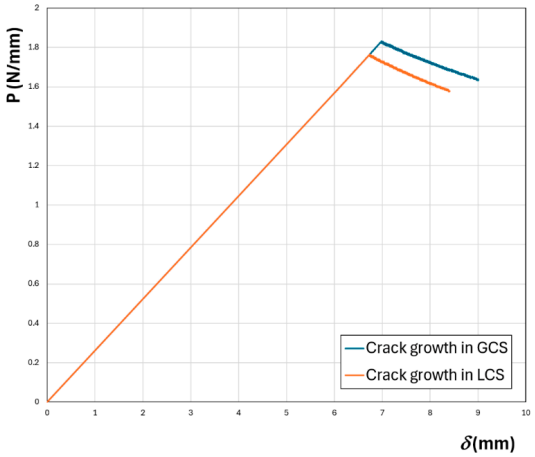


Figure 14. Crack onset and growth in global and local coordinate systems.

This finding is consistent with previous results. As G_{Ic}, G_{IIc} and η are constants, and G_T is independent of the coordinate system used for calculations, the B-K criterion evaluated in LCS and GCS only differs due to G_{II} values. As shown in Tables 5 and 6, G_{II} presents lower values when calculated in the LCS, so the B-K criterion predicts a lower critical load when evaluated in the LCS.

5. Conclusions

Since the ADCB specimen undergoes non-negligible rotations during the application of the load, this non-linearity must be taken into account in the calculation of the ERR.

This correction is not usually implemented in numerical codes or in analytical developments found in the scientific literature. This work shows that the difference in ERR results when the angle of rotation of the sample is taken into account or not (using LCS or GCS) can be significant. For an applied displacement of only 5 mm, the difference obtained in the calculation of G_I and G_{II} can reach 4% and 14%, respectively, when calculated in LCS or GCS. For an applied displacement of 10 mm, the difference obtained in G_I and G_{II} values can reach 10% and 35%, respectively.

When performing crack growth calculations, the difference between critical values (both load and displacement at the crack onset) taking, or not, into account the rotation of the sample can be in the order of 4%.

This work shows that, for ADCB samples, it is important that the ERR in modes I and II be calculated using the displacements and forces projected according to a coordinate system that rotates with the crack plane, that is, perpendicular and tangential to the crack plane, in order to obtain accurate results. This is especially important when the displacement applied to the lips of the sample and/or the difference in stiffness of the sublaminates are significant.

Author Contributions: Conceptualization, J.B. and V.M.; formal analysis, J.B. and V.M.; investigation J.B. and V.M.; methodology, J.B.; software, J.B. and V.M.; validation, J.V. and A.A.; writing—original draft preparation, J.B.; writing—review and editing V.M. All authors have read and agreed to the published version of the manuscript.

Funding: This research received no external funding.

Data Availability Statement: The original contributions presented in this study are included in the text. Further inquiries can be directed to the corresponding author.

Conflicts of Interest: The authors declare no conflicts of interest.

Abbreviations

The following abbreviations are used in this manuscript:

FEM	Finite Element Modelling
DCB	Double Cantilever Beam
ENF	End Notched Flexure
ADCB	Asymmetric Double Cantilever Beam
VCCT	Virtual Crack Closure Technique
TSEM	Two-Step Extension Method
GCS	Global Coordinate System
LCS	Local Coordinate System

References

1. *ISO 15024*; Fibre-Reinforced Plastic Composites-Determination of Mode I Interlaminar Fracture Toughness, GIC, for Unidirectionally Reinforced Materials. International Organization for Standardization: Geneva, Switzerland, 2023.
2. *ASTM D5528/D5528M-21*; Standard Test Method for Mode I Interlaminar Fracture Toughness of Unidirectional Fiber-Reinforced Polymer Matrix Composites. ASTM International: West Conshohocken, PA, USA, 2021. [CrossRef]
3. *ASTM D7905/D7905M-19e1*; Standard Test Method for Determination of the Mode II Interlaminar Fracture Toughness of Unidirectional Fiber-Reinforced Polymer Matrix Composites. ASTM International: West Conshohocken, PA, USA, 2019. [CrossRef]
4. *ASTM D6671/D6671M–22*; Standard Test Method for Mixed Mode I-Mode II Interlaminar Fracture Toughness of Unidirectional Fiber Reinforced Polymer Matrix Composites. ASTM International: West Conshohocken, PA, USA, 2022; pp. 1–15.
5. Crews, J.H.; Reeder, J.R. *A Mixed-Mode Bending Apparatus for Delamination Testing*; NASA: Washington, DC, USA, 1988; NASA Technical Memorandum 100662.
6. Ramírez, F.M.G.; de Moura, M.F.S.F.; Moreira, R.D.F.; Silva, F.G.A. Experimental and Numerical Mixed-Mode I + II Fracture Characterization of Carbon Fibre Reinforced Polymer Laminates Using a Novel Strategy. *Compos. Struct.* **2021**, *263*, 113683. [CrossRef]
7. Szekrényes, A.; Uj, J. Comparison of Some Improved Solutions for Mixed-Mode Composite Delamination Coupons. *Compos. Struct.* **2006**, *72*, 321–329. [CrossRef]
8. Szekrényes, A. Prestressed Fracture Specimen for Delamination Testing of Composites. *Int. J. Fract.* **2006**, *139*, 213–237. [CrossRef]
9. Boyano, A.; Mollón, V.; Bonhomme, J.; De Gracia, J.; Arrese, A.; Mujika, F. Analytical and Numerical Approach of an End Notched Flexure Test Configuration with an Inserted Roller for Promoting Mixed Mode I/II. *Eng. Fract. Mech.* **2015**, *143*, 63–79. [CrossRef]
10. Williams, M.L. *The Stresses Around a Fault or Crack in Dissimilar Media*; Seismological Society of America: Albany, CA, USA, 1959; Volume 49.
11. Sundararaman, V.; Davidson, B.D. An Unsymmetric Double Cantilever Beam Test for Interfacial Fracture Toughness Determination. *Int. J. Solids Struct.* **1997**, *34*, 799–817. [CrossRef]
12. Ducept, F.; Gamby, D.; Davies, P. A Mixed-Mode Failure Criterion Derived from Tests on Symmetric and Asymmetric Specimens. *Compos. Sci. Technol.* **1999**, *59*, 609–619. [CrossRef]
13. Krueger, R. Virtual Crack Closure Technique: History, Approach, and Applications. *Appl. Mech. Rev.* **2004**, *57*, 109–143. [CrossRef]
14. Chaboche, J.L.; Girard, R.; Schaff, A. Numerical Analysis of Composite Systems by Using Interphase/Interface Models. *Comput. Mech.* **1997**, *20*, 3–11. [CrossRef]
15. Chen, J.; Crisfield, M.; Kinloch, A.J.; Busso, E.P.; Matthews, F.L.; Qiu, Y. Predicting Progressive Delamination of Composite Material Specimens via Interface Elements. *Mech. Compos. Mater. Struct.* **1999**, *6*, 301–317. [CrossRef]
16. Valvo, P.S. On the Calculation of Energy Release Rate and Mode Mixity in Delaminated Laminated Beams. *Eng. Fract. Mech.* **2016**, *165*, 114–139. [CrossRef]
17. Williams, J.G. Observations on the Analysis of Mixed Mode Delamination in Composites. *Procedia Eng.* **2015**, *114*, 189–198. [CrossRef]
18. Wang, S.; Harvey, C.M. Mixed Mode Partition Theories for One Dimensional Fracture. *Eng. Fract. Mech.* **2012**, *79*, 329–352. [CrossRef]
19. VCCT-Based Crack Growth Simulation. ANSYS Release 2023R2. In *Fracture Analysis Guide 3.5*; ANSYS, Inc.: Canonsburg, PA, USA, 2023.
20. Mollón, V.; Bonhomme, J.; Elmarakbi, A.M.; Argüelles, A.; Viña, J. Finite Element Modelling of Mode I Delamination Specimens by Means of Implicit and Explicit Solvers. *Polym. Test.* **2012**, *31*, 404–410. [CrossRef]
21. Bonhomme, J.; Argüelles, A.; Viña, J.; Viña, I. Numerical and Experimental Validation of Computational Models for Mode I Composite Fracture Failure. *Comput. Mater. Sci.* **2009**, *45*, 993–998. [CrossRef]

22. Bonhomme, J.; Mollón, V.; Viña, J.; Argüelles, A. Finite Element Analysis of the Longitudinal Half Fixed Beam Method for Mode III Characterization. *Compos. Struct.* **2020**, *232*, 111546. [CrossRef]
23. Mollón, V.; Bonhomme, J.; Viña, J.; Argüelles, A. Mixed Mode Fracture Toughness: An Empirical Formulation for GI/GII Determination in Asymmetric DCB Specimens. *Eng. Struct.* **2010**, *32*, 3699–3703. [CrossRef]
24. Wang, W.; Lopes Fernandes, R.; Teixeira De Freitas, S.; Zarouchas, D.; Benedictus, R. How Pure Mode I Can Be Obtained in Bi-Material Bonded DCB Joints: A Longitudinal Strain-Based Criterion. *Compos. B Eng.* **2018**, *153*, 137–148. [CrossRef]
25. Benzeggagh, M.L.; Kenane, M. Measurement of Mixed-Mode Delamination Fracture Toughness of Unidirectional Glass/Epoxy Composites with Mixed-Mode Bending Apparatus. *Compos. Sci. Technol.* **1996**, *56*, 439–449. [CrossRef]
26. Falcó, O.; Ávila, R.L.; Tijs, B.; Lopes, C.S. Modelling and Simulation Methodology for Unidirectional Composite Laminates in a Virtual Test Lab Framework. *Compos. Struct.* **2018**, *190*, 137–159. [CrossRef]

Disclaimer/Publisher's Note: The statements, opinions and data contained in all publications are solely those of the individual author(s) and contributor(s) and not of MDPI and/or the editor(s). MDPI and/or the editor(s) disclaim responsibility for any injury to people or property resulting from any ideas, methods, instructions or products referred to in the content.